PERGAMON

International Journal of Heat and Mass Transfer 42 (1999) 2525–2541

International Journal of HEAT and MASS TRANSFER

Numerical prediction of heat and momentum transfer over micro-grooved surface with a nonlinear k–ε model

Moktar Benhalilou, Nobuhide Kasagi*

Department of Mechanical Engineering, The University of Tokyo, Hongo 7-3-1, Bunkyo-ku, Tokyo 113-8656, Japan

Received 13 December 1996; in final form 30 October 1998

Abstract

The paper reports numerical results obtained in a fully developed turbulent channel flow with triangular riblets. The heat and momentum transfer characteristics are calculated by using a nonlinear low-Reynolds number k–ε model together with several turbulent scalar flux representations. Comparison of the drag variation prediction with previous experimental and numerical data shows that the present turbulence model can simulate the turbulent flow over this complex surface reasonably well. By comparing the results obtained with the isotropic and anisotropic Reynolds stress representations, the significance of the mean secondary flow in the drag reduction mechanism is discussed. In both drag reducing and increasing conditions, the drag change predicted is found to be in close agreement with the data available in the literature. Under the drag reducing conditions, possible departure from the Reynolds analogy is investigated at various Reynolds and Prandtl numbers. It is shown that, while the skin friction is reduced over the riblet surface, the heat transfer performance can actually be increased beyond that on a smooth wall, although discrepancy with the experimental data is not negligible.

Nomenclature

C_f skin friction coefficient $= 2\tau_w/(\rho U^2_b)/\cos\alpha$
c_p specific heat at constant pressure
H channel height
h riblet height, unless otherwise denoted
k turbulent kinetic energy
Nu Nusselt number $= hH/\lambda$, where h denotes the heat transfer coefficient
P_k shear production of k $(= -\overline{u_i u_j} U_{i,j})$
Pr Prandtl number, ν/κ
Pr_t turbulent Prandtl number, ν_t/κ_t
p static pressure
q_w heat flux averaged on the wall surface
R shear parameter $= k/(S\nu)$
Re Reynolds number $= U_b H/\nu$
Re_τ Reynolds number $= u_\tau \delta/\nu$
St Stanton number $= q_w/(\rho c_p U_b \Theta_b)/\cos\alpha$
s riblet spacing
U_i ith component of mean velocity
U_b bulk mean velocity
u_i ith component of fluctuating velocity
u_τ friction velocity on the smooth wall.

Greek symbols

α ridge angle (see Fig. 1)
δ channel half width $= H/2$
δ_{ij} Kronecker delta
ε dissipation rate of turbulent kinetic energy
Θ mean scalar
θ fluctuating scalar
κ thermal diffusivity
κ_t turbulent thermal diffusivity
λ thermal conductivity
ν kinematic viscosity
ν_t turbulent kinematic viscosity
ρ density
σ_k turbulent Prandtl number of k
σ_ε turbulent Prandtl number of ε
τ_w shear stress averaged on the wall surface.

Subscripts

b bulk mean

* Corresponding author. Tel.: +81 3 3812 2111; fax: +81 3 5800 6999.
E-mail address: kasagi@thtlab.t.u-tokyo.ac.jp (N. Kasagi)

0017–9310/99/$ - see front matter
PII: S0017–9310(98)00348–2

r riblet wall
s smooth wall
t turbulent
w at the wall surface
i partial derivative with respect to x_i.

1. Introduction

The control of the near-wall coherent structures is of great importance for various engineering applications. It has become evident that these structures are responsible for the turbulent momentum and scalar transport, especially in the vicinity of a solid wall [1–3]. As underlined by Hamilton et al. [4], the turbulence is sustained by a self-regenerating process. Starting from this observation, one can imagine that once we are able to alter or disrupt the cycle of regeneration, effective turbulence control techniques can be developed. A very attractive issue is whether it is possible to obtain a wall geometry that reduces a skin friction coefficient, while enhancing a heat transfer coefficient. If it is possible, such wall geometry would be particular advantageous in reduction of friction drag and noise, improvement in aerodynamical performance, and reduction of the volume, weight and even fabrication costs of various heat transfer equipment, to name a few.

A wall surface with micro-grooves, so-called riblets, aligned in the flow direction presents the advantage of reducing the drag, while increasing the surface area in contact with the fluid compared with a smooth wall. Up to 8% reduction in the drag has been obtained by Walsh [5] in laboratory experiments, while in flight conditions 1–2% reduction has been reported [6]. Hence, this type of surface geometry might possibly increase the Reynolds analogy factor beyond that on a smooth wall. Although experimental measurements are extremely difficult over the micro-grooved surfaces, a few attempts at NASA Langley [7, 8] concluded that heat transfer augmentation would be possible under drag reducing conditions and for moderate molecular Prandtl number fluids.

Although the riblets are recognized as a successful device, at least, for the drag reduction purpose, the mechanism responsible is not fully clear and neither true optimization nor improvement of the method has been made up to the present. Recently, very pointwise flow field measurements have been performed over and within the riblets [9–11] ([11] is referred to as SK, hereafter). It is worth recalling, however, that both heat and momentum transfer takes place in a thin layer just above the wall, where uncertainties in experimental measurement are usually very large. Hence, if we rely only on experiments, the understanding of heat and momentum transfer mechanisms over riblet surfaces should be difficult, and the optimization of the wall geometry that provides the least skin friction coefficient and the largest heat transfer coefficient would be almost impossible.

Recently, Chu and Karniadakis [12] and Choi et al. [13] (CMK, hereafter) have applied successfully DNS to the turbulent flow over the riblets. The results of these studies are consistent, at least qualitatively, with the experimental data available and have extended our knowledge about the turbulence structure over this complex surface. CMK even predicted the drag variation in accordance with Walsh's results [5].

However, when considering the heat transfer prediction, the refinement of the grid system is important for high molecular Prandtl number fluids. Hence, a parametric study by DNS, which is relatively costly and requires large computer resources, is hardly possible. Furthermore, only low-Reynolds number flows, which are not representative of most of the real conditions, can be explored. Then, numerical computation with a turbulence model should be an alternative. Its cost is moderate compared with that of experiments or DNS even at high Reynolds numbers. In addition, a parametric study can be carried out very easily, in which both mean field parameters and some of the turbulent statistics are calculated. Launder and Li [14] adopted the Launder and Sharma model [15] (LS, hereafter), which makes appeal neither to the distance to the wall, nor to the shape of the solid boundary, but only to the local turbulent Reynolds number. The study has shown that, while the computed mean field over triangle riblets agrees fairly well with the experimental data, the turbulent field does not. A difficulty in predicting correctly the drag variation has also become evident.

In the present study a low-Reynolds number k–ε model is adopted. In order to predict the turbulent heat and momentum transfer over the riblets, some preliminary requirements have to be satisfied. Firstly, it is well known that most of the two-equation models reproduce the wall proximity effect by referring to the wall distance. Because it is not straightforward to define the wall distance over non-flat surfaces, this notion becomes hard to use. Thus, it is highly desirable to use a two-equation model which is completely free from the wall topography. To the authors knowledge, two of the current k–ε models satisfy this requirement: the LS model and that recently developed by Yang and Shih [16] (YS, hereafter). In the present study, the latter model is employed, and comparison with the former is made. Secondly, DNS [13] and experiments [11] have reported the existence of mean secondary flow in the plane normal to the main flow direction. The anisotropy of the normal stresses in the corner region originates this secondary flow. Then, the nonlinear stress representation developed by Myong and Kasagi [17] has been adopted. It is expected to predict the mean secondary flow and to help to assess its significance in the heat and momentum transfer mechanisms over riblets. Finally, in order to compute the scalar field, several scalar

flux models of different level of sophistication are used [18–20].

In the present paper, the capability of the selected nonlinear two-equation model to predict accurately the drag variation is explored. Then, heat and momentum transfer characteristics are presented in the close vicinity of the triangular wall. Based on the numerical results, an analysis is given of the effects of several mechanisms that could be involved in the heat and momentum transfer. It shows that viscous retardation of the flow inside the groove, the mean secondary flow and the reduction of the thermal layer thickness for high Prandtl number fluids should be the main contributors to the observed heat and momentum modification induced over triangular riblet walls.

2. Turbulence models

2.1. Dynamic field

With the assumption of an incompressible and stationary flow, the Reynolds-averaged Navier–Stokes equations can be written in the Cartesian coordinates as:

$$U_j\frac{\partial U_i}{\partial x_j}=-\frac{1}{\rho}\frac{\partial p}{\partial x_i}+\frac{\partial}{\partial x_j}\left(\nu\frac{\partial U_i}{\partial x_j}-\overline{u_iu_j}\right) \tag{1}$$

$$\frac{\partial U_i}{\partial x_i}=0. \tag{2}$$

where U_i and u_i are the ith components of the mean and fluctuating velocities.

The YS k–ε model is given as:

$$U_j\frac{\partial k}{\partial x_j}=\frac{\partial}{\partial x_j}\left(\left(\nu+\frac{\nu_t}{\sigma_k}\right)\frac{\partial k}{\partial x_j}\right)+P_k-\varepsilon \tag{3}$$

$$U_j\frac{\partial \varepsilon}{\partial x_j}=\frac{\partial}{\partial x_j}\left(\left(\nu+\frac{\nu_t}{\sigma_\varepsilon}\right)\frac{\partial \varepsilon}{\partial x_j}\right)+\frac{C_{\varepsilon_1}P_k-C_{\varepsilon_2}\varepsilon}{T_t}+E \tag{4}$$

where $\nu_t=C_\mu f_\mu kT_t$, $T_t=k/\varepsilon+(\nu/\varepsilon)^{1/2}$, $C_\mu=0.09$, $C_{\varepsilon1}=1.44$, $C_{\varepsilon2}=1.92$, $\sigma_k=1.0$, $\sigma_\varepsilon=1.3$, and $E=\nu\nu_t U_{i,jk}^2$, respectively. At a high Reynolds number, the time scale of turbulence T_t reduces to k/ε, and in the near-wall region, to the Kolmogorov time scale $(\nu/\varepsilon)^{1/2}$. This choice of two scales is equivalent to the original idea of Myong and Kasagi [21].

The damping function is expressed as:

$$f_\mu=(1-\exp(-a_1R-a_2R^2-a_3R^3))^{1/2} \tag{5}$$

where $R=k/(S\nu)$, with S being the modulus of the strain rate tensor $S=(2S_{ij}S_{ij})^{1/2}$ and $S_{ij}=0.5(U_{i,j}+U_{j,i})$. The constants a_1, a_2 and a_3 are given as 3×10^{-4}, 6×10^{-5} and 2×10^{-6}, respectively. As the local state of the flow is the basis for representing the wall proximity effect, the ambiguity in the definition of the wall distance is avoided.

In order to investigate whether the mean secondary flow in the plane normal to the main flow direction is sustained near the riblets [11, 13], the following anisotropic stress representation [17] is adopted:

$$\frac{\overline{u_iu_j}}{k}=\frac{2}{3}\delta_{ij}-\frac{\nu_t}{k}\left(\frac{\partial U_i}{\partial x_j}+\frac{\partial U_j}{\partial x_i}\right)+\frac{\nu_t}{\varepsilon}\sum_{\beta=1}^{3}C_\beta\left(S_{\beta ij}-\frac{\delta_{ij}}{3}S_{\beta\alpha\alpha}\right)+\frac{2\nu}{3\varepsilon}W_{ij}\left[\left(\frac{\partial\sqrt{k}}{\partial y}\right)^2+\left(\frac{\partial\sqrt{k}}{\partial z}\right)^2\right] \tag{6}$$

where

$$S_{1ij}=\frac{\partial U_i}{\partial x_\gamma}\frac{\partial U_j}{\partial x_\gamma}$$

$$S_{2ij}=\frac{1}{2}\left(\frac{\partial U_\gamma}{\partial x_i}\frac{\partial U_j}{\partial x_\gamma}+\frac{\partial U_\gamma}{\partial x_j}\frac{\partial U_i}{\partial x_\gamma}\right)$$

$$S_{3ij}=\frac{\partial U_\gamma}{\partial x_i}\frac{\partial U_\gamma}{\partial x_j}$$

$$W_{ij}=-\delta_{ij}+(\delta_{i2}\cos\alpha+\delta_{i3}\sin\alpha)\times(\delta_{j2}\cos\alpha+\delta_{j3}\sin\alpha)+4\delta_{i1}\delta_{j1}.$$

The constants in the model are $C_1=0.8$, $C_2=0.45$ and $C_3=-0.15$, respectively, and α denotes the ridge angle of the triangular riblet (see Fig. 1). Although the original constants values of C_β were optimized in plane channel flows, they are kept unchanged as a first approximation. In the near-wall region, the third term on the right-hand side of Equation (6) vanishes and becomes negligible compared with the fourth term which represents the wall limiting behavior of the Reynolds stresses. The formulation of W_{ij} in Equation (6) has been modified from that originally proposed in order to take into account the wall normal on the riblet surface. On the opposite smooth wall, the ridge angle α is zero, and the formulation switches back to the original.

2.2. Thermal field

The thermal field is solved by:

$$U_j\frac{\partial\Theta}{\partial x_j}=\frac{\partial}{\partial x_j}\left(\frac{\nu}{Pr}\frac{\partial\Theta}{\partial x_j}-\overline{u_j\theta}\right)+\frac{Q}{\rho c_p} \tag{7}$$

in which the source term Q is constant, and the wall surfaces are at a constant temperature.

The turbulent Prandtl number correlation of Myong and Kasagi [18], which is a function of the molecular Prandtl number, Pr, was adopted:

$$-\overline{u_j\theta}=\frac{\nu_t}{Pr_t}\frac{\partial\Theta}{\partial x_j} \tag{8}$$

$$Pr_t=0.75+\frac{1.63}{\ln(1+Pr/0.0015)}. \tag{9}$$

Equation (9) is consistent with the theoretical behavior over a wide range of Pr and is proportional to $1/Pr$ for $Pr\ll1$ over a conventional smooth wall. However, in the case of a non-circular duct, the turbulent Prandtl number and local heat transfer coefficient increase as a corner is

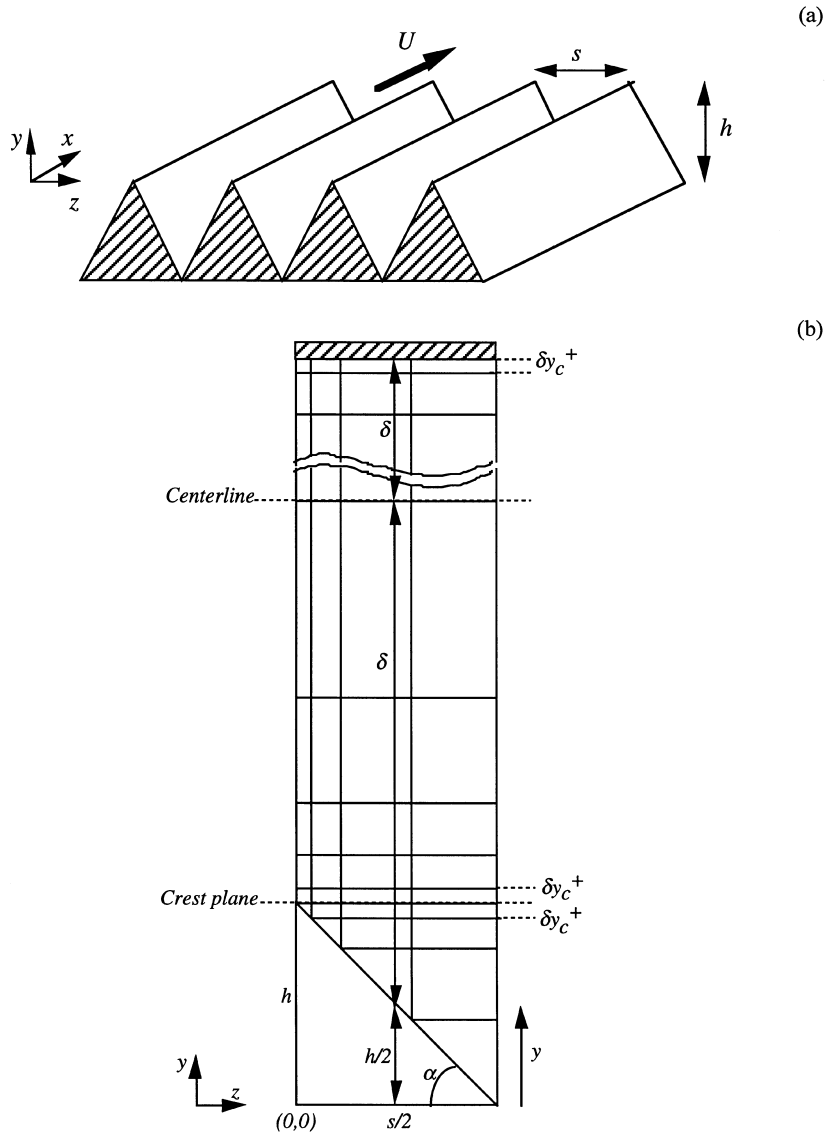

Fig. 1. General view of a riblet plate and coordinates system.

approached [22]. Obviously, Equation (9) can not account for this phenomenon, and the turbulent Prandtl number assumption might underestimate the heat transfer efficiency of the riblet surfaces. Then, two additional more sophisticated turbulence models, i.e., the General Gradient Diffusion Hypothesis (GGDH) [19] and the WET model [20] are introduced. They are respectively given as:

$$-\overline{u_j\theta} = c_\theta \frac{k}{\varepsilon} \overline{u_j u_k} \frac{\partial \Theta}{\partial x_k} \tag{10}$$

$$-\overline{u_j\theta} = c_\theta \frac{k}{\varepsilon} \left(\overline{u_j u_k} \frac{\partial \Theta}{\partial x_k} + \overline{u_k \theta} \frac{\partial U_j}{\partial x_k} \right), \tag{11}$$

where c_θ is equal to 0.3.

3. Computational domain and boundary conditions

In order to reduce the computation load, a fully developed turbulent channel flow is investigated. The flow field and thermal field do not vary in the streamwise direction, which simplifies the formulation to a pseudo-tridimensional problem. The computation domain is reduced to a single station that is normal to the mean streamwise direction. It is an asymmetric channel (Fig. 1). One wall is mounted with a riblet surface, while the other remains smooth. The channel half-height δ is set to be 20 times the riblet height h, unless stated otherwise. The computations are performed for two different geometric ratios, i.e., $s/h = 1$ and 2, and for the Reynolds

Table 1
Characteristics of the grid system

	Riblet peak	Riblet valley
δy_c^+	0.09	0.47
Number of points within $y^+ \leqslant 5$	23	13

$Re = 5600$, $h^+ \approx 9$.

number Re which varies from 3000 to 20 000. The grid system is refined in the vicinity of the crest in order to determine the steep velocity and temperature gradients with high accuracy. The first grid points above the crest plane and above the smooth wall are located at the same distance, well within the viscous sublayer. In case of a smooth channel flow, grid independent results are obtained with about 100 points distributed over the channel height. The minimum grid spacing δy_c is selected so that its further reduction does not change appreciably the ratio of the velocity gradients $(U_{,n})_{crest}/(U_{,n})_{smooth}$, where n denotes the normal direction. Doubling the number of grid points in both the normal and spanwise directions inside the groove gives about 1% variation in the skin friction coefficient over the riblet (at $h^+ = 10 = hu_\tau/\nu$, $s/h = 2$). Note that all nondimensionalization denoted by superscript + are made using the friction velocity relative to the smooth wall throughout the paper. Table 1 summarizes some characteristics of the grid system in the vicinity of the riblet wall, for the case $h^+ = 9$. A very fine grid is used within the viscous sublayer ($y^+ < 5$) with the first grid point always located within $y^+ < 1$. The number of grid points is 191×40 along the y- and z-directions. In the y-direction, 40 of the 191 points are located within the riblet valley and the rest between the crest plane and the smooth wall.

At the symmetry planes ($z = 0$ and $s/2$, in Fig. 1), the antisymmetric condition is used for the normal component, and for all other variables, the normal gradient is given to be zero. At the walls, all the variables are zero, except the dissipation rate of the turbulent kinetic energy, for which $\varepsilon_w = \nu k_{,nn}$.

4. Flow field

Among various possible physical mechanisms that contribute to the observed drag variation, the strong viscous effect is often cited. In laminar boundary layer, Djenidi et al. [23] pointed out that the strong viscous effect that generates retardation of the mean flow inside the riblet might compensate the increase of the wetted area and under certain flow conditions provide a small amount of drag reduction. However, they did not confirm the conclusion from experimental measurements. In the case of a body of revolution mounted with a riblet surface, Schneider and Dinkelacker [24] reported no effect on the drag. In a channel flow configuration, a consensus seems to indicate that the riblet surfaces increase the drag [12, 25, 26]. Although conflicting results are obtained, it seems likely that, due to the low-speed or stagnant fluid within the valley induced by viscosity, the drag penalty is not in relation with the considerable increase of the wetted area. In turbulent flows, experiments [9–11] and DNS [12–13] have shown a similar retardation of the flow inside the riblet valley, which is believed to be caused by viscosity. However, additional effects are expected to explain the turbulent friction drag variations.

In the next section, riblet performances under various flow conditions are given. A comparison with experimental data enables to discuss the capability of the present turbulence model to reproduce this complex flow. Then, based on the numerical results, a detailed analysis of the structural change in the flow field over riblet surfaces is presented.

4.1. Performance of riblets

In Fig. 2, the relative change of the skin friction coefficient compared to that without the riblets is shown as a function of h^+. Note that h^+ increases from about 5 to 28 as Re increases from 3000 to 20 000. Due to the measurement uncertainties and the turbulence model, perfect agreement is not possible, but the present anisotropic model is able to predict the trend and the magnitude of the experimental results reasonably well.

For both ratios of s/h, the present computations predict the greatest reduction about $h^+ = 10 \sim 15$. However, for large riblet spacing ($s/h = 2$), the range of h^+ which provides reduction is somewhat larger than indicated by the experimental data. Compared with the LS model prediction (dashed lines), an improvement of the optimum flow condition (h^+) is obtained. Indeed, it is now well established that riblets surfaces would provide drag reduction for riblet height below $h^+ = 30$, which is below LS model predictions. This improvement suggests that the shear parameter (R) in the YS model function may be more suitable than the turbulent Reynolds number alone for capturing the rapid change and the strong inhomogeneity in the close vicinity of the riblets. In addition, at low Reynolds number, the LS model produces a thickening of the viscous sublayer. Then, the skin friction coefficient is underestimated, and the magnitude of drag reduction might be overestimated.

In order to estimate the significance of the mean secondary flow in the drag variation, the isotropic eddy viscosity model is used for comparison. The mean secondary flow is hardly observed, and its intensity is found very weak. The isotropic model gives worse agreement

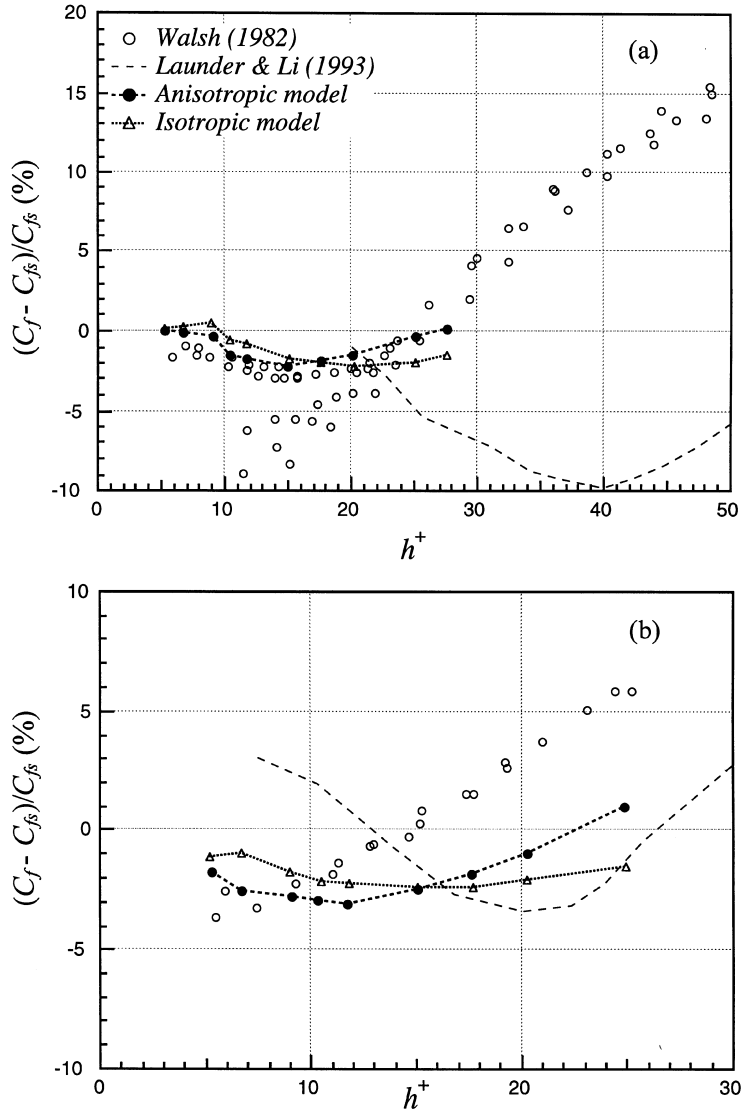

Fig. 2. Skin friction coefficient variation over riblets: (a) $s/h = 1$, (b) $s/h = 2$.

with the experimental data than the anisotropic model. Below the range $h^+ = 15 \sim 17$, the action of the mean secondary flow would tend to reduce the skin friction, while beyond this range, it would tend to increase it appreciably. However, the net influence of the mean secondary flow seems limited and can not explain by itself the differences observed between laminar and turbulent skin friction variations. It is worth noting that when using the isotropic model, the optimum flow condition is obtained at a higher Reynolds number than with the anisotropic model.

4.2. Flow field structure

The flow structure change is examined below by comparing two different flow conditions. They correspond to the drag reducing and increasing conditions of the CMK DNS [13]. The geometric ration s/h is 2, and the Reynolds number, $Re_\tau = u_\tau \delta/\nu$, is 180. In this section only, the ratio of the channel height to the riblet height H/h is changed, so that two different flow conditions, $h^+ = 10$ and 20, are simulated. In the present work, about 3% reduction and 1% increase in the turbulent skin friction are obtained

for $h^+ = 10$ and 20, respectively, while 2% reduction and 3% increase in Walsh [5].

In Fig. 3, the contour diagram of the streamwise velocity normalized by the centerline velocity is given. The increment between two successive isolines represents $U/U_c = 0.1$. One can observe that the spanwise inhomogeneity of the streamwise velocity is confined to the near-wall region, in very good agreement with SK.

Bacher and Smith [27] conjectured that the mean secondary flow might be caused by the interaction of the near-wall streamwise vortices with the riblet surface and would bring momentum from the valley region toward the rib peak. The present result is plotted in Fig. 4. For $h^+ = 10$, the center of the eddy is located slightly above the crest plane, while it is deeper within the groove for $h^+ = 20$. For $h^+ = 10$, the maximum intensity is about 0.25% of the centerline velocity. When $h^+ = 20$, it reaches about 2%, strengthening the mechanism of momentum transfer described above. Less intense eddies have been observed by CMK and SK. In both studies, the eddies are obtained by averaging instantaneous secondary velocity fields over a sufficiently long period. The authors observed that, in the drag increasing case, the mean secondary flow is more intense than in the drag reducing case, and this is in good agreement with the present results.

The Reynolds shear stress is plotted in Fig. 5. The present YS model is seen to reproduce fairly well this quantity over the smooth wall in accordance with the data of Kim et al. [28] (KMM, hereafter). Note that the

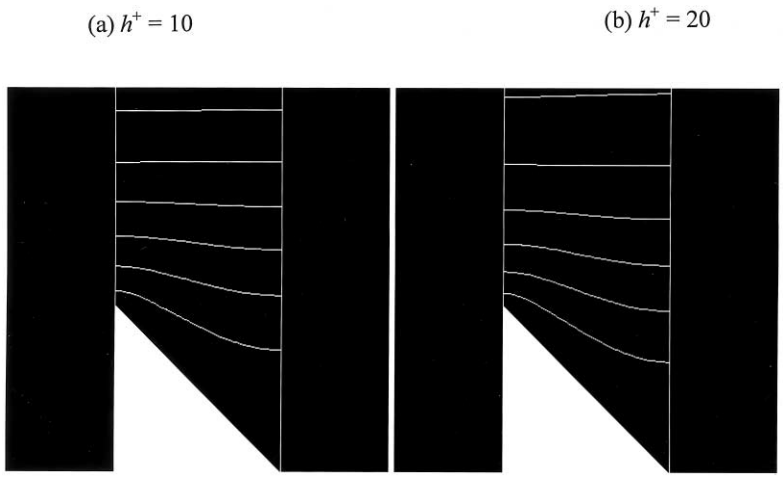

Fig. 3. Contours of streamwise velocity: (a) $h^+ = 10$, $s/h = 2$; (b) $h^+ = 20$, $s/h = 2$.

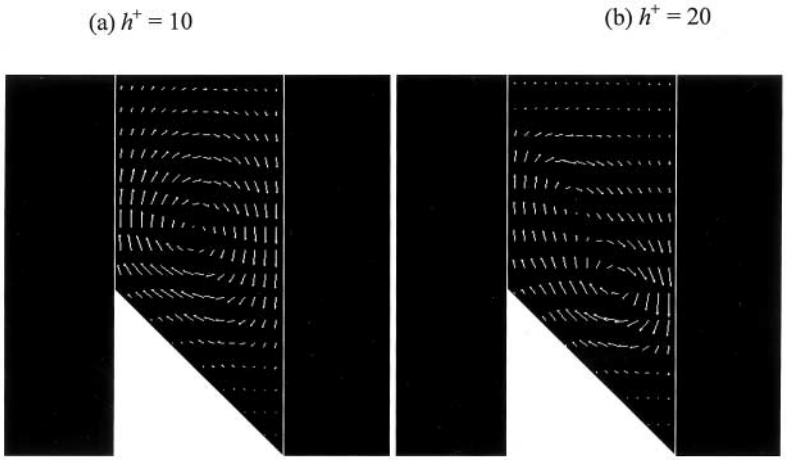

Fig. 4. Mean secondary flow in the y–z plane: (a) $h^+ = 10$, $s/h = 2$; (b) $h^+ = 20$, $s/h = 2$.

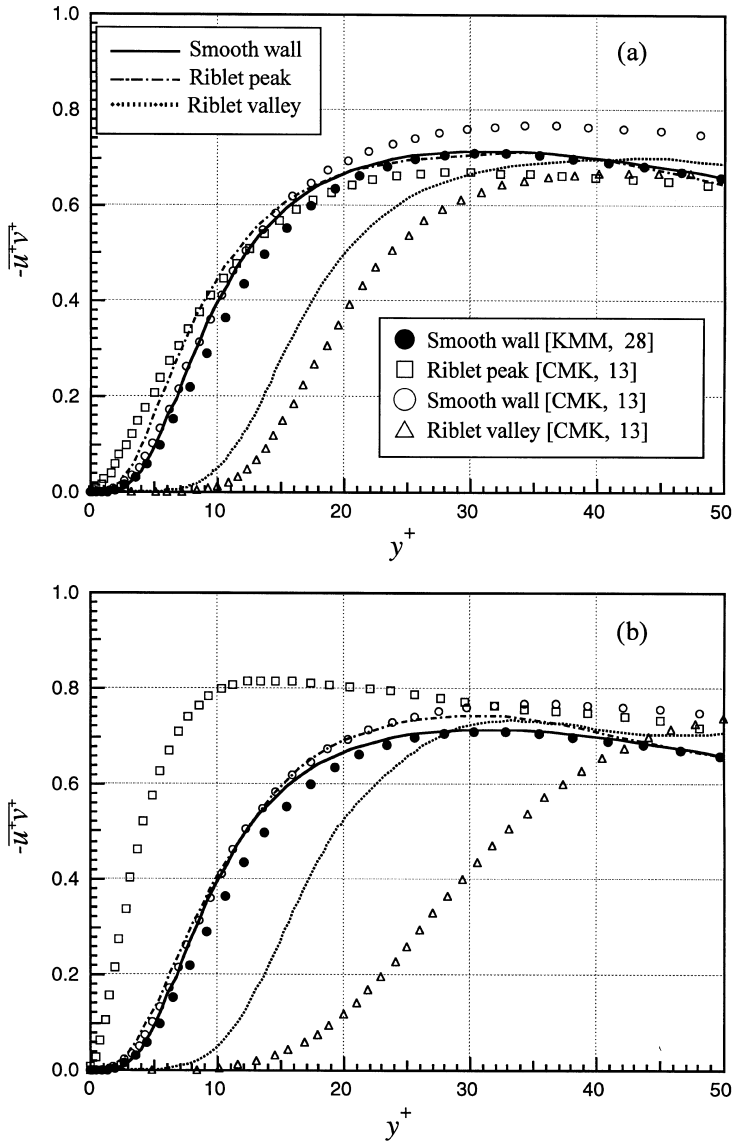

Fig. 5. Reynolds shear stress: (a) $h^+ = 10$, $s/h = 2$; (b) $h^+ = 20$, $s/h = 2$.

smooth wall data of CMK differs from that of KMM. This should be owing to the relatively small computational domain of CMK, i.e., the so-called minimal flow unit, and to their grid system which is coarse in the streamwise direction. When drag is reduced ($h^+ = 10$), the modification of the stress distribution is predicted generally well. The maximum Reynolds shear stress is decreased above the riblets, i.e., about 1.5 and 2.5% reduction above the crest and valley, respectively. CMK reported 12% reduction in the maximum shear stresses over the riblets. The spanwise variation of the maximum stress is very small in both studies. The experimental results of SK indicate about 15% reduction in the Reynolds shear stress in close agreement with the CMK data.

For $h^+ = 20$, the Reynolds shear stress is increased over the riblet; about 5 and 2.5% above the crest and valley, respectively, as shown in Fig. 5(b). These results are somewhat conflicting with those of CMK above the valley position, but they are in good agreement with the experimental results of SK.

Based on the numerical results, two different features are conjectured in these profiles. When $h^+ = 10$, the flow is very little sheared inside the riblets, suggesting dynamical inactivity. It could correspond to the fact that the

near-wall coherent vortices, whose diameter is about $d^+ = 30$, can not intrude deep inside the riblets due to the small spacing ($s^+ = 20$) as described by SK and CMK. These structures interact only with the rib peak area, where the wall shear stress is largely enhanced. When $h^+ = 20$, the near-wall coherent structures are free to penetrate inside the riblets ($s^+ = 40$) and interact with a large area of the riblet surface. The flow inside the groove becomes dynamically active.

The turbulent kinetic energy is shown in Fig. 6 Over the smooth wall, the agreement with the KMM data is relatively poor. The maximum is overestimated, but located at the same position. For $h^+ = 10$, the turbulent kinetic energy is reduced above the riblets, but discrepancies exist with the data of CMK. For $h^+ = 20$, the maximum of the turbulent kinetic energy is obtained above the rib valley, unlike CMK's results.

5. Thermal field

Fig. 7 shows a comparison of the computed mean temperature profiles in a smooth channel, for the Prandtl number ranging from 0.10 to 2.0, with the DNS of Kim and Moin [29]. Equation (9) gives turbulent Prandtl numbers of 1.14, 1.01 and 0.98 for $Pr = 0.10$, 0.71 and 2.00,

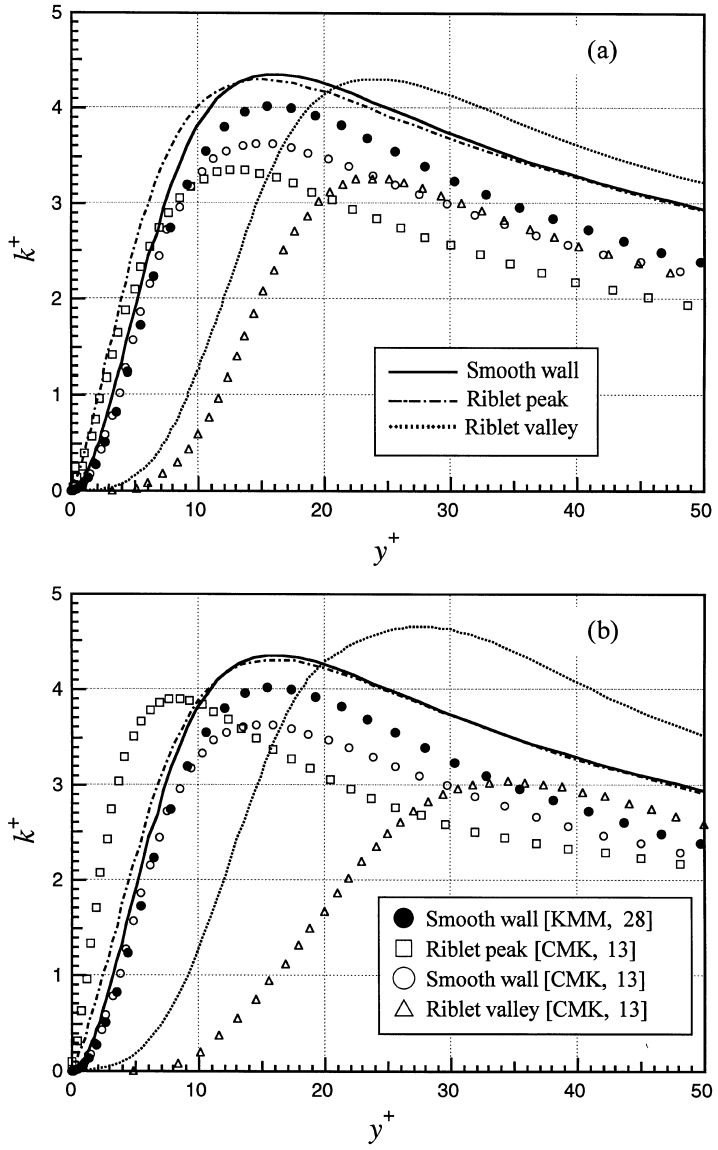

Fig. 6. Turbulent kinetic energy: (a) $h^+ = 10$, $s/h = 2$; (b) $h^+ = 20$, $s/h = 2$; lines and symbols as in Fig. 5.

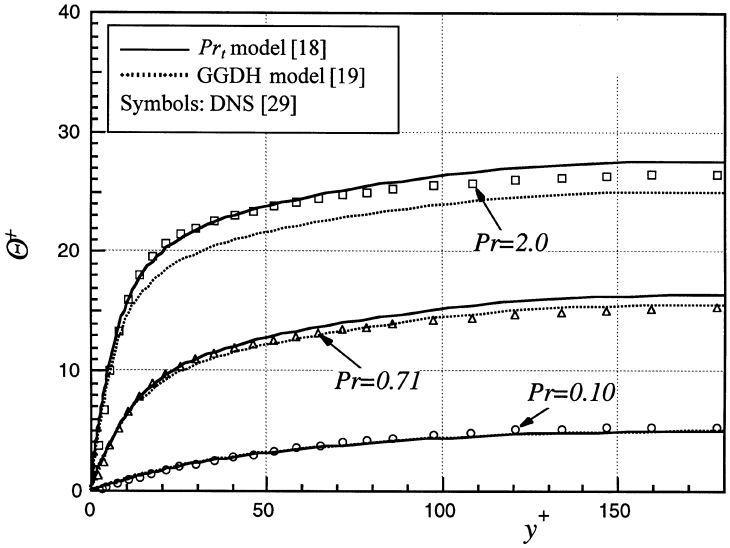

Fig. 7. Temperature profiles in a smooth channel flow.

respectively. These values remain quite close to those obtained in DNS. With both the turbulent Prandtl number and the GGDH model, the temperature profiles shown good consistency with DNS in the near-wall region. Further away from the wall, a departure from the reference profile is notable for high Prandtl number fluids.

5.1. Heat transfer efficiency of riblet surfaces

Figs 8 and 9 show the heat transfer efficiency of the riblet surface, which is defined as:

$$\eta = \frac{(q_w/\tau_w)_r}{(q_w/\tau_w)_s} = \frac{(2St/C_f)_r}{(2St/C_f)_s}, \tag{12}$$

where q_w, τ_w and St are the heat flux, the shear stress and the Stanton number averaged on the wall, and the subscripts r and s denote the quantities on the riblet and smooth walls, respectively. For both values of s/h, the efficiency of the riblets becomes smaller than unity at low Pr. The relative heat transfer rate on the riblet surface is smaller than that on the smooth wall.

When both Prandtl and Reynolds numbers are sufficiently large, the riblet efficiency becomes larger than the smooth wall one. As expected, among the three models used (Pr_t, GGDH and WET), the turbulent Prandtl number assumption gives the smallest efficiency.

At $Pr = 0.7$, present computation indicates at worse 15% reduction (Pr_t) and at best 10% improvement (WET model) in heat transfer efficiency. For similar experimental flow conditions, Walsh and Weinstein [7] and Lindemann [8] obtained up to 10 and 35% increase in heat transfer efficiency. The reason for the discrepancy between experimental and numerical results is not completely clear to the present authors. However, the experimental results should be used with caution, since simultaneous drag and heat transfer measurements are extremely difficult over micro-grooved surfaces. In addition, it is hard to find physical arguments in favor of such large heat transfer augmentation at $Pr = 0.7$ in fully developed thermal boundary layers.

The heat transfer efficiency of the riblet increases with the geometric ratio s/h (Figs 8 and 9), and the limit between loss and gain is moving toward lower Prandtl numbers. However, when s/h increases excessively, the riblet surfaces becomes closer from the smooth wall, and the benefit on drag is reduced quickly.

5.2. Thermal field structure

Generally speaking, at low Pr, the velocity and temperature contours appear similar (not shown here). Hence, one can expect close similarity in the momentum and heat transfer processes. In Fig. 10, the spanwise variation of the local Nusselt number is plotted. For both geometric ratios at $Pr = 0.71$, the large increase of the Nusselt number around the riblet peak ($z/s = 0$) is counterbalanced by the important decrease inside the valley ($z/s = 0.5$). In contrast, for high Pr, a large reduction of the thermal layer thickness occurs. Its dimension which is of the order of the channel half-height for low Pr, reduces now considerably to become of the order of the riblet height. The local Nusselt number becomes larger inside the valley, and the whole riblet surface, of which area is much greater than the smooth wall, contributes to the heat transfer augmentation (Fig. 10). This is especially right for the GGDH and WET

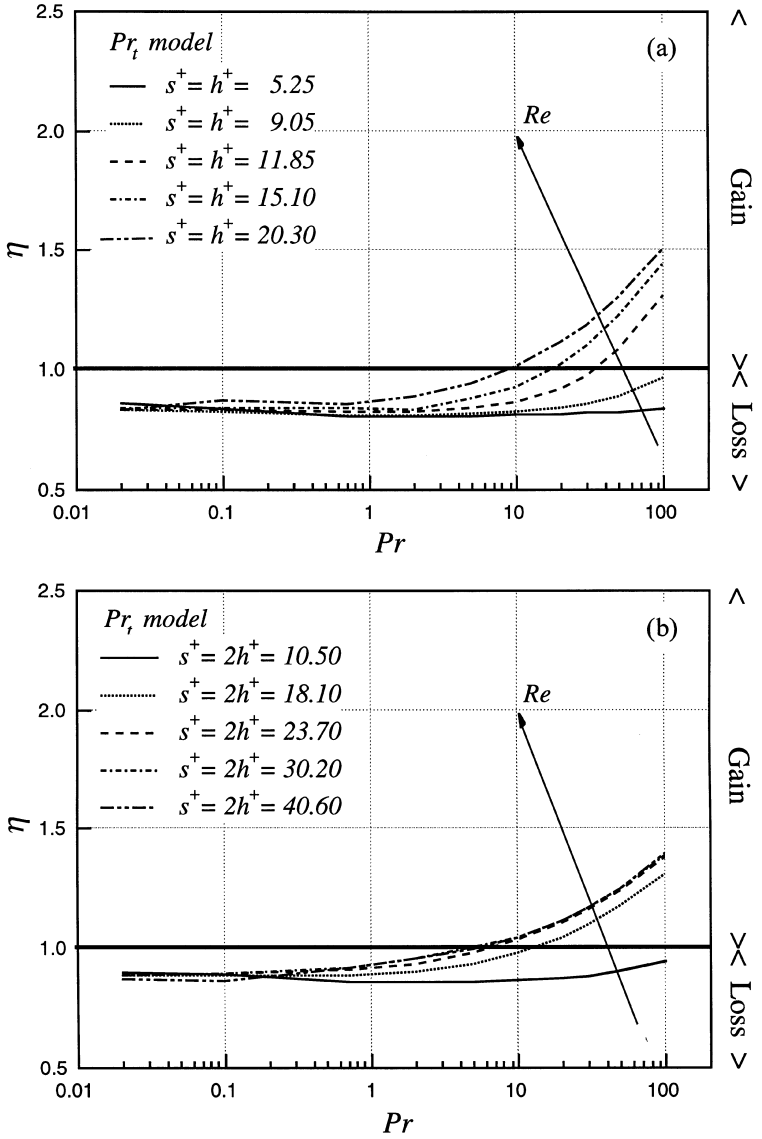

Fig. 8. Heat transfer efficiency of the riblet surfaces (Pr_t model): (a) $s/h = 1$, (b) $s/h = 2$.

models, which give much larger increase of the efficiency than the turbulent Prandtl number assumption.

5.3. Role of the mean secondary flow

Since there exists a considerable mixing due to the mean secondary flow inside the groove, we turn our attention to its effect on the heat transfer efficiency. The following discussion focuses on the case of large riblet spacings ($s/h = 2$), for which the influence of the mean secondary flow is the most pronounced. Figure 11 shows the temperature contours with and without the mean secondary flow under the same flow conditions (Re and Pr). The temperature is normalized by the centerline temperature, and the increment between two successive isolines represents $\Theta/\Theta_c = 0.1$. For low Pr, the mean secondary flow is embedded in a thermal layer of larger thickness. Very close to the wall, the temperature convected by the mean secondary flow has little influence on the thermal field (Fig. 11(a) and (b)). As Pr increases, the thermal layer thickness becomes very small compared to the dimensions of the vortices. Due to induced convection, high temperature fluid is transported away from the solid wall around the riblet peak. Within the valley, high

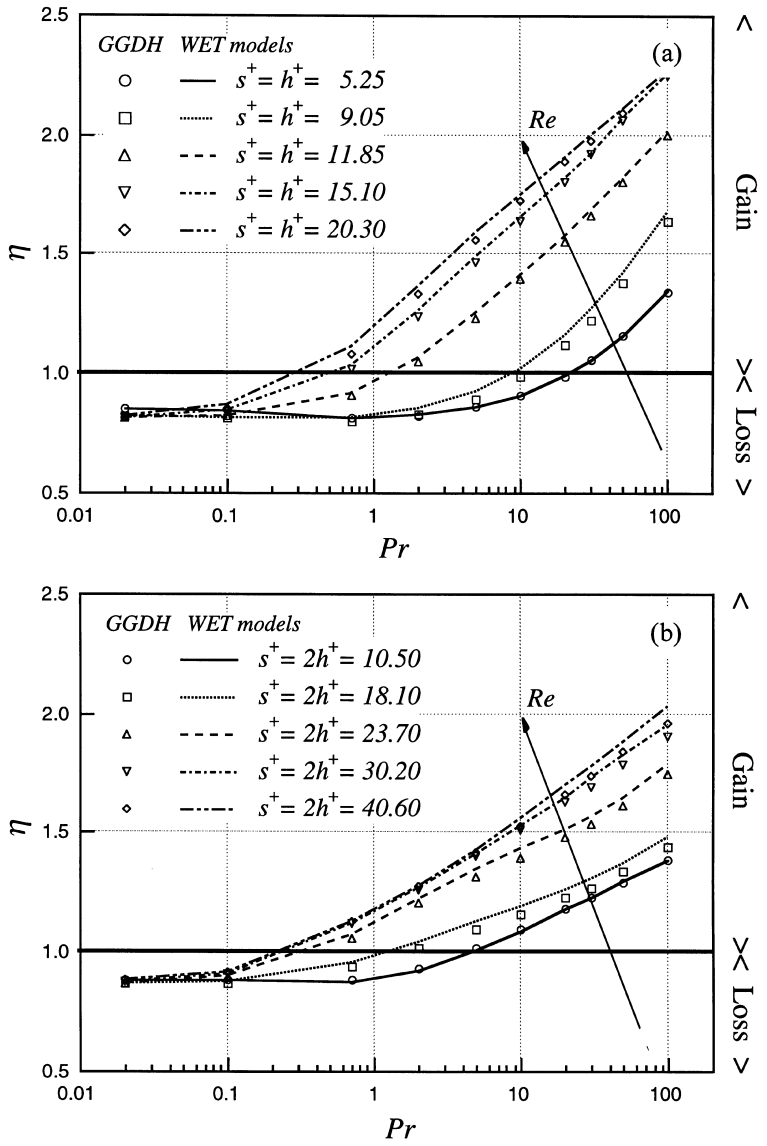

Fig. 9. Heat transfer efficiency of the riblet surfaces (GGDH model): (a) $s/h = 1$, (b) $s/h = 2$.

temperature fluid is pushed toward the wall. This feature is remarkable in Fig. 11(d), where the temperature contours are strongly buckled.

Figure 12 gives a comparison of the spanwise variation of the local Nusselt number obtained with and without the mean secondary flow. These results are obtained with the turbulent Prandtl number assumption. For low Pr, the action induced is almost negligible, and very little change is visible on the profile. For high Pr, with the vigorous influence of the mean secondary flow, the local Nusselt number increases in the valley and decreases above the riblet peak, in particular for $s/h = 2$, as indicated by arrows in Fig. 12(b).

Heat transfer efficiencies obtained with the isotropic eddy viscosity model are given in Fig. 13. For low Pr, the effect of the mean secondary flow on the heat transfer efficiency is negligible (see Figs 8 and 9). For high Pr, about 20% of the total gain would result from it (at $Re = 5600$ for $Pr = 100$), with the turbulent Prandtl number assumption. By using the GGDH model, this gain is about 10%.

6. Conclusions

The turbulent heat and momentum transfer over a riblet surface was investigated by using a nonlinear k–ε

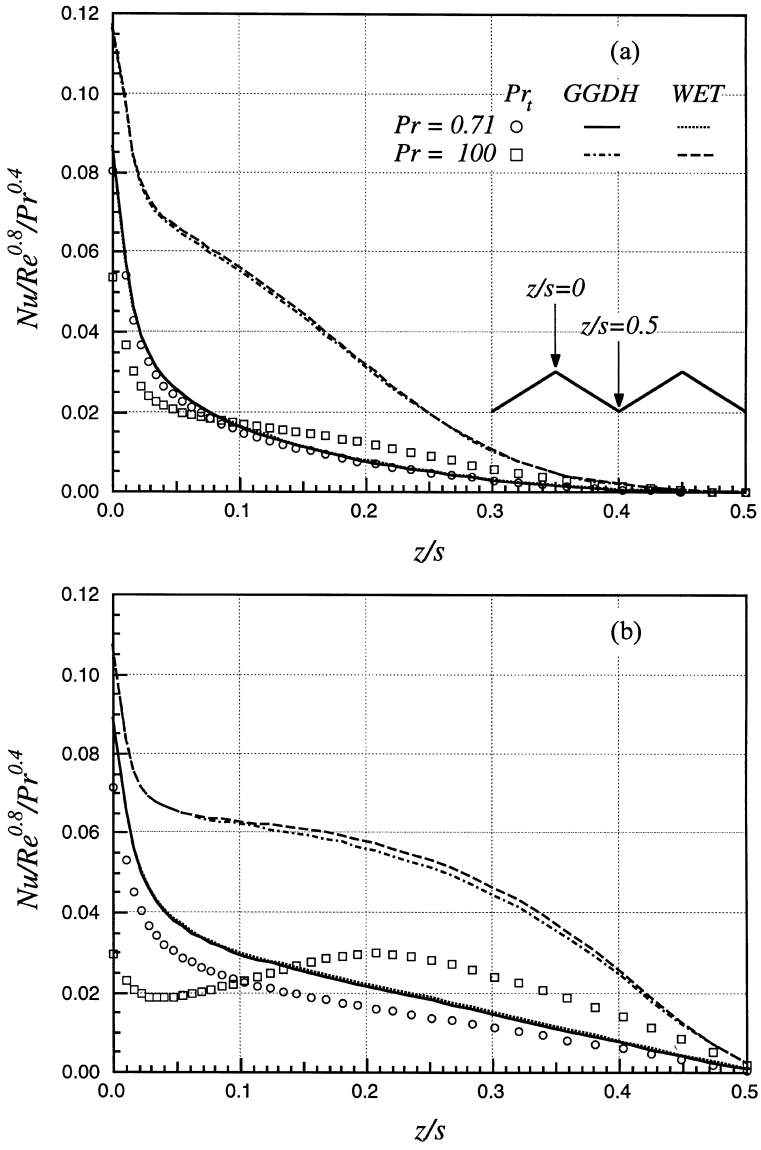

Fig. 10. Distribution of the local Nusselt number along the riblet wall ($Re = 5600$, $h^+ = 9$): (a) $s/h = 1$, (b) $s/h = 2$.

model, which consists of the model of Yang and Shin [16] together with the anisotropic stress representation developed by Myong and Kasagi [17]. Several scalar flux representations have been used to close the scalar transport equation [18–20]. The present work aimed at: (1) testing one of the actual two-equation turbulence model for the prediction of turbulent flow over triangle riblet surfaces; (2) investigating possible heat transfer augmentation; (3) based on these numerical results, trying to better understand the drag reduction and heat transfer augmentation mechanisms induced by these complex surfaces.

The drag variations computed at various Reynolds numbers show good consistency with the Walsh data [5], mainly at small h^+. In particular, the predicted optimum flow condition remains very close to that of experiments. The major advantages of the turbulence model adopted are the abandonment of the reference to the wall topography, and the implementation of the shear parameter in the model function. This latter seems to be more suitable than the turbulent Reynolds number alone (i.e., LS model) in capturing the complex flow over the riblets.

Furthermore, the anisotropic representation for the Reynolds stress is shown to be indispensable for the prediction of turbulent flows over such complex surfaces. On a hand, it allowed us to predict the mean secondary

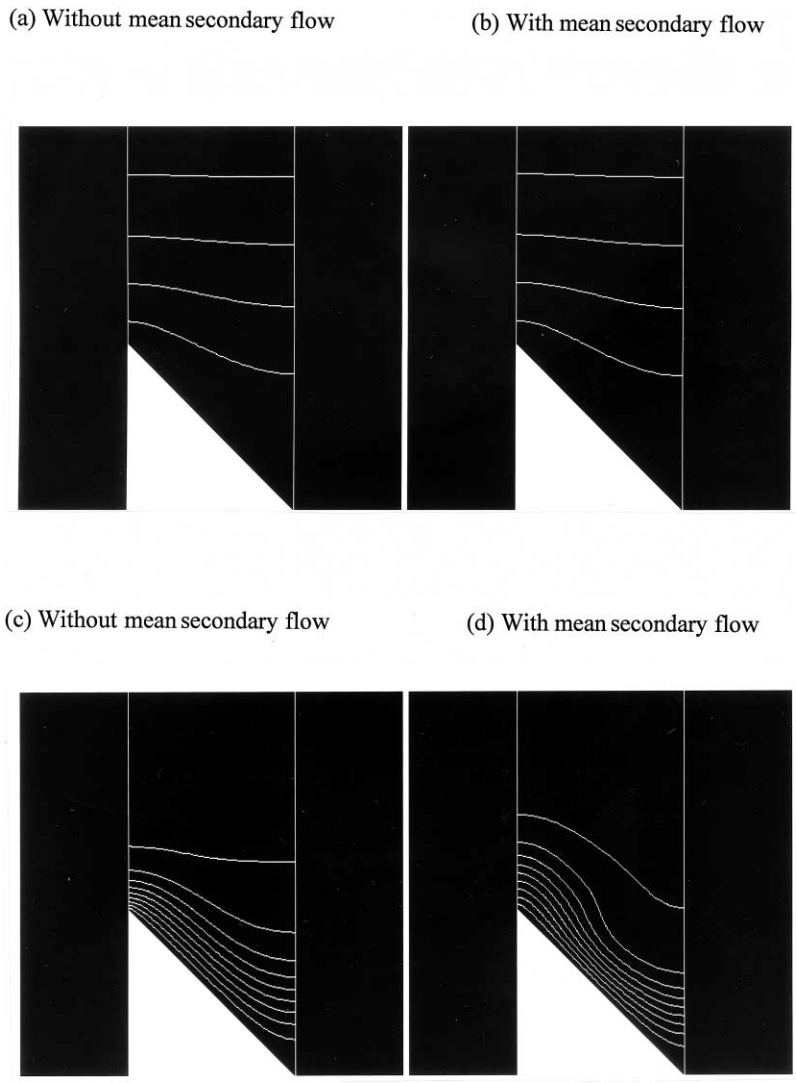

Fig. 11. Contours of temperature with and without the mean secondary flow ($Re = 5600$, $h^+ = 9$, $s/h = 2$): (a) and (b): low Prandtl number; (c) and (d): high Prandtl number.

flow that exists in the plane normal to the mean flow direction. Although the dynamic of these vortices remains so far unclear, these vortices contribute to the inhomogeneity of the flow field in the close vicinity of the riblet surfaces. The present study shows a contribution of a few percent to the total reduction/augmentation of the skin friction. On the other hand, its presence is also necessary for the determination of the optimal flow condition. In particular, it is demonstrated that by suppressing it, the optimal flow condition is shifted toward higher h^+.

Under drag reducing conditions, an increase of the heat transfer efficiency might be possible, departing from the Reynolds analogy principle. However, the present results are somewhat conflicting with the previous experimental works of Welsh and Weinstein [7] and Lindemann [8]. The heat transfer efficiency increase is observed mainly for high Prandtl number fluids, whereas their experiments indicated a very large increase for air flow.

The origin of the heat transfer augmentation lies in the large reduction of the thermal layer thickness that occurs for higher Pr. In that case, the whole riblet area is contributing to the heat transfer. For riblets such as $s/h = 2$, it represents about 40% increase of the area. For low Pr, only the riblet peak vicinity contributes to the heat transfer processes and it becomes difficult to achieve a drastic improvement compared with the smooth wall.

Finally, it is shown that the mean secondary flow is

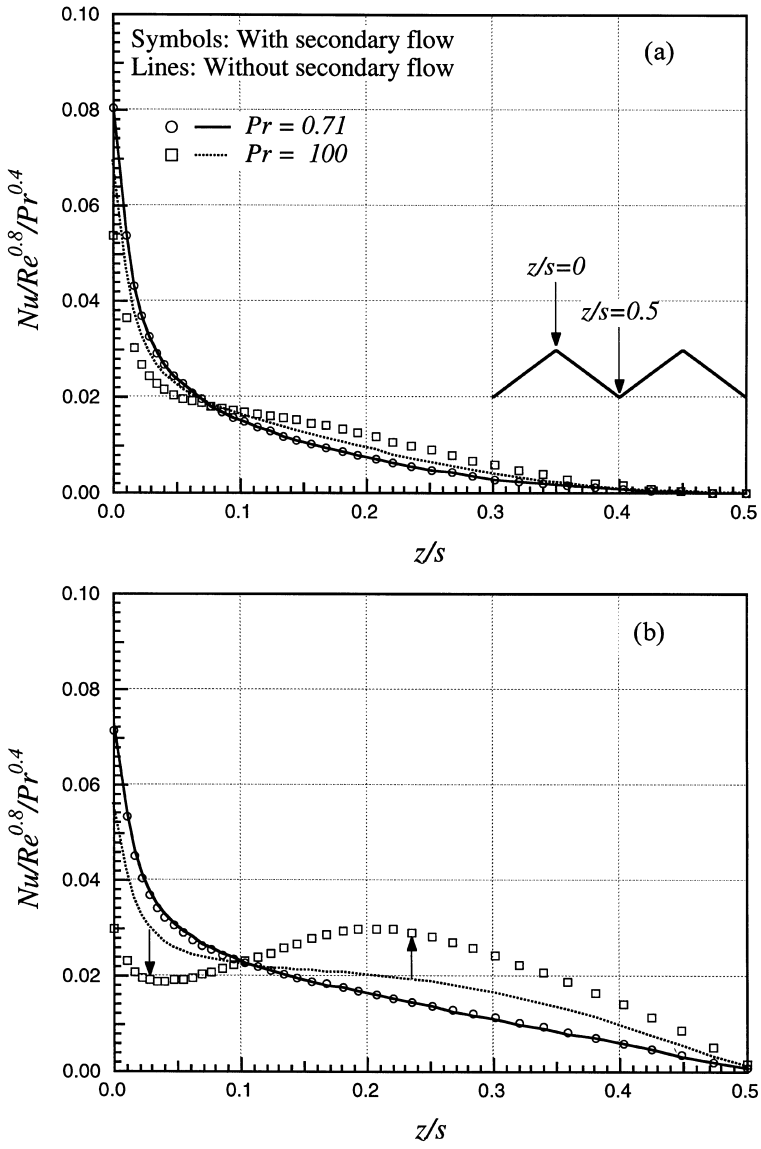

Fig. 12. Distribution of the local Nusselt number along the riblet wall with and without the mean secondary flow ($Re = 5600$, $h^+ = 9$): (a) $s/h = 1$, (b) $s/h = 2$.

also an important factor in the heat transfer mechanism. With its action, enthalpy is convected near the wall, and the global heat transfer efficiency is affected. However, this occurs mainly for high Pr fluids, when the dimension of the mean secondary vortices is large enough compared with that of the thermal layer thickness.

Since the momentum and heat transports are closely related, improvement of the two-equation models is necessary and the development of anisotropic models that are able to capture the strong flow field inhomogeneity would be of great help, if one aims at optimizing the wall geometry that provides the least skin friction coefficient and the largest heat transfer coefficient by numerical simulation.

Acknowledgements

The authors acknowledge the financial support through the Grant-in-Aid for Scientific Research on Priority Areas (No. 05240103) by the Ministry of Education, Science and Culture. Dr. M. Benhalilou thanks the Japan

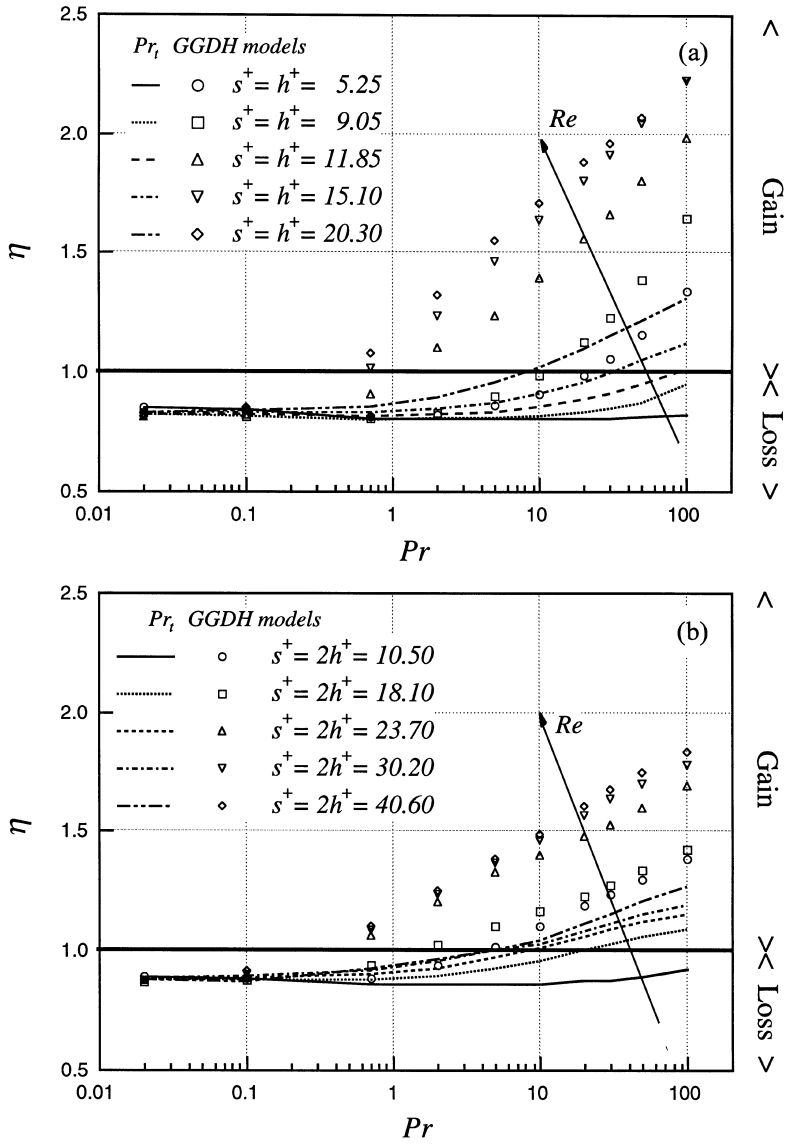

Fig. 13. Efficiency of the riblet surfaces without the mean secondary flow: (a) $s/h = 1$, (b) $s/h = 2$.

Society for the Promotion of Science (JSPS) for supporting his stay at the University of Tokyo during the course of this work.

References

[1] S.K. Robinson, Coherent motions in the turbulent boundary layer structure, Annual Review of Fluid Mechanics 23 (1991) 601–639.

[2] N. Kasagi, Y. Ohtsubo, Direct numerical simulation of low Prandtl number thermal field in a turbulent channel flow, in: F. Durst, R. Friedrich, B.E. Launder, F.W. Schmidt, U. Schumann, J.H. Whitelaw, (Eds.), Turbulent Shear Flow, vol. 8, Springer-Verlag, Berlin, 1993, pp. 97–119.

[3] N. Kasagi, Y. Sumitani, Y. Suzuki, O. Iida, On the kinematics of the quasi-coherent vortical structure in near-wall turbulence, Int. J. Heat Fluid Flow 16 (1) (1995) 2–10.

[4] J.M. Hamilton, J. Kim, F. Waleffe. Regeneration of near-wall turbulence structures, Proceedings of the Eighth Symposium on Turbulent Shear Flows, Kyoto Japan, 1993, pp. 1151–1156.

[5] M.J. Walsh, Turbulent boundary layer drag reduction using riblets, AIAA Paper No. 82-0169, 1982.

[6] J.P. Robert, Drag reduction: an industrial challenge, Proceedings of Special Course on Skin Friction Drag Reduction, Brussels, AGARD-VKI, 1992.

[7] M.J. Walsh, L.M. Weinstein, Drag and heat transfer characteristics of small longitudinally ribbed surfaces, AIAA J. 17 (1979) 770–771.
[8] A.M. Lindemann, Turbulent Reynolds analogy factors for nonplanar surface microgeometries, J. Spacecraft 22 (1985) 581–582.
[9] P. Vukoslavcevic, J.M. Wallace, J.L. Balint, Viscous drag reduction using streamwise aligned riblets, AIAA J. 30 (1992) 1119–1122.
[10] M. Benhalilou, F. Anselmet, L. Fulachier, Conditional Reynolds stress on a V-grooved surface, Phys. Fluids 6 (1994) 2101–2117.
[11] Y. Suzuki, N. Kasagi, On the turbulent drag reduction mechanism above a riblet surface, AIAA J. 32 (1994) 1781–1790.
[12] D.C. Chu, G.E.M. Karniadakis, A direct numerical simulation of laminar and turbulent flow over riblet-mounted surfaces, J. Fluid Mech. 250 (1993) 1–42.
[13] H. Choi, P. Moin, J. Kim, Direct numerical simulation of turbulent flow over riblets. J. Fluid Mech. 255 (1993) 503–539.
[14] B.E. Launder, S.P. Li, On the prediction of riblet performance with engineering turbulence models, Appl. Sci. Res. 50 (1993) 283–298.
[15] B.E. Launder, B.I. Sharma, Application of the energy dissipation model of turbulence to the calculation near a spinning disc, Letters in Heat and Mass Transfer 1 (1974) 131–138.
[16] Z. Yang, T.H. Shih, A Galilean and tensorial invariant k–ε model for near-wall turbulence, AIAA Paper No 93-3105, 1993.
[17] H.K. Myong, N. Kasagi, Prediction of anisotropy of the near-wall turbulence with an anisotropic low-Reynolds number k–ε model, ASME J. Fluids Eng. 112 (1990) 521–524.
[18] H.K. Myong, N. Kasagi, Numerical prediction of turbulent pipe flow heat transfer for various Prandtl number fluids with the improved k–ε model, JSME Int. J. Series II 32 (1989) 613–622.
[19] B.J. Daly, F.H. Harlow, Transport equations of turbulence, Phys. Fluids 13 (1970) 2634–2649.
[20] B.E. Launder, On the computation of convective heat transfer in complex turbulent flows, ASME J. Heat Transfer 110 (1988) 1112–1128.
[21] H.K. Myong, N. Kasagi, A new approach to the improvement of k–ε turbulence model for wall-bounded shear flow, JSME Int. J. Series II 33 (1990) 63–72.
[22] M. Hirota, H. Fujita, H. Yokosawa, H. Nakai, H. Itoh, Turbulent heat transfer in a square duct, Proceedings of the Engineering Foundation Conference on Turbulent Heat Transfer, San Diego, California, U.S.A., 1996.
[23] L. Djenidi, F. Anselmet, J. Liandrat, L. Fulachier. Laminar boundary layer over riblets, Phys. Fluids 6 (1994) 2993–2999.
[24] M. Schneider, A. Dinkelacker, Drag reduction by means of surface riblets on an inclined body of revolution, in: R.M.C. So, C.G. Speziale, B.E. Launder (Eds.), Near-Wall Turbulent Flows, Elsevier, New York, 1993, pp. 771–780.
[25] B.E. Launder, S.P. Li, A numerical study of riblets effects on laminar flow through a plane channel, Appl. Sci. Res. 46 (1989) 271–280.
[26] H. Choi, J. Kim, P. Moin, On the effect of riblets in fully developed laminar channel flows, Phys. Fluids 3 (1991) 1892–1896.
[27] E.V. Bacher, C.R. Smith, A combined visualization–anemometry study of the turbulent drag reduction mechanism of triangular micro-groove surface modification, AIAA Paper No. 85-0548, 1985.
[28] J. Kim, P. Moin, R. Mozer, Turbulent statistics in fully developed channel flow at low-Reynolds number, J. Fluid Mech. 177 (1987) 133–166.
[29] J. Kim, P. Moin, Transport of passive scalar in a turbulent channel flow, in: J.C. André, J. Cousteix, F. Durst, B.E. Launder, F.W. Schmidt, J.H. Whitelaw, (Eds.), Turbulent Shear Flow, vol. 6, Springer–Verlag, Berlin, 1989, pp. 85–96.